ACTA METALLURGICA SLOVACA
2024, VOL. 30, NO. 2, 90-99

RESEARCH PAPER

THE SIMULATION OF THE ANISOTROPY OF ALUMINUM ALLOY SHEETS BY DEEP DRAWING: A CRUCIAL STUDY FOR THE AUTOMOTIVE AND MATERIALS ENGINEERING INDUSTRIES

Emil Spišák[1], Janka Majerníková[1], Peter Mulidrán[1], Július Hajduk[1], František Ruda[1]*

[1] Institute of Technology and Materials Engineering, Faculty of Mechanical Engineering, Technical University of Košice, Mäsiarska 74, 040 01 Košice, Slovakia; janka_majernikova@tuke.sk; peter.mulidran@tuke.sk; julius.hajduk@student.tuke.sk, frantisek.ruda@student.tuke.sk

*Corresponding author: emil.spisak@tuke.sk, tel.: +421556023502, Faculty of Mechanical Engineering, Technical University of Košice, Mäsiarska 74, 040 01 Košice, Slovakia

Received: 03.06.2024
Accepted: 04.06.2024

ABSTRACT

Recently, the automotive industry has shown an increasing interest in utilizing thin aluminum alloy sheets to reduce the weight of various car components. The occurrence of uneven cup heights in deep drawing processes is called earing. This issue arises due to the planar anisotropy of sheets, a consequence of crystallographic texture. Therefore, this study involves a meticulously conducted cylindrical cupping test. For the experimental research, four different aluminum alloys were used, each with distinct mechanical and plastic properties. The experimental results of the drawing process were compared with the simulation results using the Simufact Forming software. Different numbers of elements were selected for experimental material with a 1 mm thickness to further compare the simulation results with experiments. In a separate simulation in the Simufact Forming software, the effect of the number of elements on the earing height and computing time was evaluated. The results obtained with five different solvers were compared within Simufact Forming. The results showed significant differences in computing times for the different types of solvers.

Keywords: deep drawing, aluminum alloy sheets, earing, simulation, Simufact Forming

INTRODUCTION

Because of its face-centred cubic lattice, aluminum is very suitable for hot and cold forming. Cold working can increase its strength, but it decreases its plastic properties [1]. Aluminum's resistance to weather conditions is due to its ability to form an adhesive layer of aluminum oxide on its surface, which prevents oxidation [2, 3].

When examining the strength-to-weight ratio, aluminum alloys outperform steel, with a greater advantage in favor of aluminum. Additionally, aluminum alloys offer the advantage of higher toughness at low temperatures compared to steel. However, they have a drawback in terms of lower fatigue strength, which can be enhanced by adding chemical elements like V, Ti, and Zr [4-6]. The chemical composition-based classification of aluminum alloys is defined by EN 573-3:2019-12 [7], which categorizes them into eight classes ranging from 1xxx to 8xxx [7, 8].

The European automotive industry has invented and implemented several innovative solutions related to low-weight advanced aluminum alloys [9-11]. It has also achieved better optimization of car design, which is more aluminum-centric. Aluminum's fundamental advantages include its availability in various shaped castings, sheets, and extrusions adequately targeted for mass production and new innovative ideas. Highly integrated compact parts meet demanding requirements for high quality, high performance, and cost-effective manufacturability.

In the automotive industry, aluminum sheet is commonly used to create lightweight car body assemblies. All the different parts of the body structures must be joined together. The most used methods of joining aluminum parts are welding, resistance welding, brazing, soldering, and friction stir welding [12].

One of the most complicated processes in metal forming is the stamping process, especially the deep drawing process. Its complexity is determined by the fact that different stress-strain states are operating at the same point in the part from the beginning of the process to its completion. This effect results in different values of the pressing wall thickness, which are influenced precisely by the distribution of plastic deformations during the deep drawing process [13, 14].

The theory of forming, or also referred to as the theory of plasticity, forms the base of metal forming processes. This phenomenological theory is created based on the analytical or mathematical description of the behavior of the material continuum during plastic deformation. In addition to its various tasks, the theory of forming is concerned with analysing the deformations occurring during forming processes, the main objective of which is determining the appropriate shape and dimensions of the starting part. In multi-step operations, it is necessary to determine the shape and dimensions of the parts for each phase of the process. The limit states of plastic operations are also described by using forming theory, which determine the exceeding of the plasticity of the material and the occurrence of formed part failure [13, 15, 16].

The prediction of formability in sheet-metal stamping components is crucial in various metal-related sectors, including the automotive and aerospace industries. Anisotropy, which

influences the extent to which a sheet can be stretched in different directions, is one of the most critical and complex factors in assessing sheet metal deformation. This spatial variation in mechanical properties is typically induced by the sheet manufacturing process, such as rolling. Tools or methods that can effectively assess the extent of this unbalanced distortion would unquestionably be invaluable and enhance the technical competitiveness of manufacturers. One of the most prominent visual indicators of material anisotropy in sheet metal forming is the occurrence of "earring," especially during cylindrical cup drawing [17]. However, projecting earring profiles for highly anisotropic materials is known to be a challenging task. Subsequently, various calculation tools, whether in the analytical or numerical domain, have been the subject of study and development. Implementing analytical models requires significantly less computational effort than numerical ones. Yoon has created and continuously refined analytical models for estimating earring profiles [18].

During the same period, Chung demonstrated favorable results using analytical functions based on simple tension properties like R values and yield stresses to determine the earring profile of highly anisotropic materials [19]. Conversely, the numerical approach, such as finite element analysis (FEA), is considered more accurate because it can directly account for the effects of anisotropic plastic deformation [20]. Hill's established anisotropic yield criterion from 1948 is one of the most original and widely utilized methods for addressing orientation-dependent deformation in sheet metal during finite element simulations [21, 22]. Several decades later, Barlat introduced another model known as Yld2004-18p [23]. It is recognized that this model is a more suitable choice for predicting plastic deformation in highly anisotropic materials, as it necessitates the consideration of up to 18 mechanical properties obtained from various sheet directions [24, 25].

The Von Mises yield function is the most employed isotropic yield model, appreciated for its straightforward mathematical formulation. This simplicity makes it convenient for theoretical analysis and finite element (FE) calculations. However, owing to its underlying isotropic assumption, the Von Mises yield function falls short in describing anisotropic materials, notably in the context of sheet metal. As a result of multiple cycles of rolling and heat treatment, sheet metals develop a texture characterized by a fibrous structure and a preferred crystallisation orientation, which leads to evident anisotropic behavior [26–29].

Numerous anisotropic yield functions have been introduced to capture the anisotropic deformation characteristics of materials. Among these, the quadratic anisotropic yield function, commonly referred to as the Hill48 yield function, proposed by Hill [30], has gained widespread recognition and utilization due to its straightforward mathematical formulation [31–33]. Nevertheless, the Hill48 quadratic yield function is limited in explaining only four test outcomes. It falls short of adequately describing the "abnormal" yield behaviour observed in certain processes involving rolled sheet metals. Consequently, this model may not always be sufficient to accurately represent real physical processes when employing the conventional parameter acquisition method. However, an alternative parameter determination approach may yield different outcomes in terms of the accuracy of the yield criteria [34–36].

In addition to Hill's quadratic yield model, various other anisotropic yield models have been developed. For instance, the well-known plane stress yield function, Yld2000-2d, was introduced by Barlat et al. [37] to characterize the anisotropic plastic deformation in sheet metals, particularly for aluminum alloys. The Yld2000-2d yield function entails eight parameters that can be determined based on yield stresses and r-values at 0°, 45°, 90°, and the equibiaxial tension direction [38,39]. However, in finite element (FE) simulations, solid elements, which are necessary for some thick sheet metals, especially when the stress in the normal direction within the sheet plane is significant, cannot be employed with the Yld2000-2d yield function, as it exclusively considers plane stress variants. Barlat et al. proposed another yield function, the Yld2004, featuring 18 parameters, which can predict the occurrence of six or eight earrings [40–42].

Previous research has primarily focused on investigating the impact of yield criteria. In this context, Chung and Shah [43] conducted finite element (FE) simulations for both cup drawing and bulge tests of AA2008-T4. Given the complexity of the cup drawing process, which encompasses compression, tension, stretching, bending, and unbending conditions, they utilized data from tensile and compression tests. The calibration of the yield criterion was based on the average of these two datasets, using the Yld91 criteria. The results indicate that these criteria yielded satisfactory approximations.

Yoon and colleagues [44] explored the impact of the shape of the yield surface and the translation of its center on predicting earing defects in the AA2008-T4 alloy by employing the Yld96 yield criterion. Their findings underscored the significance of both the shape and center translation of the yield surface in predicting ear formation. Similarly, Yoon and colleagues [45] and Yoon and colleagues [46] conducted analogous investigations for earing prediction in AA2090-T3 aluminum alloys but used different yield criteria. Their work emphasized the yield criterion's critical role and the back stress translation.

In a separate study, Yoon and colleagues [47] conducted finite element simulations for the AA5042-H2 alloy, utilizing the CPB06ex2 and Yld2000-2D yield criteria. Notably, Yld2000-2D failed to accurately predict the number of ears, whereas CPB06ex2 yielded more precise results. Consequently, the importance of choosing the yield criterion was highlighted, particularly for highly anisotropic materials.

Vladimirov [48] utilized multiplicative decomposition formulations, which involve the disintegration of the deformation gradient into elastic and inelastic components. They applied the Hill48 yield criterion to anticipate earing behavior in two distinct aluminum alloys.

Similarly, Chatti and Chtioui [49] incorporated the Hill48 yield criterion alongside the kinematic hardening rule to assess the earing profile of the AA2090-T3 alloy. They observed enhanced prediction performance when considering the kinematic hardening rule.

Vrh and colleagues [50] employed the BBC2008 yield criterion and the next increment corrects error method to predict earing defects in aluminum alloys, specifically AA5042-H2 and AA2090-T3. They found that this constitutive model effectively dealt with highly anisotropic materials.

Park and Chung [51] conducted numerical analyses of the cup drawing process using the Hill48 and Yld2000-2d criteria in a separate study. They applied the associated flow rule (AFR) to the AA2090-T3 and AA5042 aluminum alloys, exhibiting 6 and 8 ears, respectively, in physical processes. The Yld2000-2d criterion, when used in conjunction with the AFR, yielded accurate approximations in line with experimental results.

Othmen [52] assessed the impact of work hardening and anisotropy on strain distribution and the accuracy of punch force-displacement predictions in the reverse deep drawing process. They utilized Mises and Hill48 yield criteria combined with isotropic and combined hardening rules. All the plasticity models successfully predicted the punch force response during the initial drawing stage. In the subsequent stage, the evolution of the punch force was discovered to be contingent on the definition of the yield locus, while the strain distribution was notably influenced by the hardening characteristics.

Grillo and colleagues [53] introduced novel stress update algorithm schemes specifically for the backward Euler and forward Euler methods to improve earing prediction accuracy and reduce

solution times. Their results, compared with conventional approaches, showed good agreement.
Similarly, Izadpanah [54] studied the AA3105 aluminum alloy, employing the Hill48 and BBC2003 criteria. They emphasized the significant impact of the choice of the yield function on the study's outcomes.
Feng and colleagues [55] devised a micromechanical constitutive model incorporating a definition of back stress at the slip system level to predict earing defects in the AA6022-T4 aluminum alloy. They also incorporated a macro-mechanical homogeneous anisotropic hardening model and conducted a comparative analysis of the numerical results. Their findings indicated that the developed micromechanical model incurred higher computational costs, whereas the macro-mechanical model resulted in shorter CPU solution times. These principles can also be used when joining by forming, such as e.g. clinching [56].
More recently, Habraken [57] extensively investigated various parameters, encompassing yield criteria, flow rules, hardening rules, friction, stress update schemes, and more, to assess their impact on earing prediction performance.
The paper discusses the influence of drawing conditions and mechanical properties on the anisotropy of aluminum, which are manifested by the formation of ears on the cylindrical cups. The real measured earing of the cylindrical cups was compared with the numerical simulation obtained using Simufact software. Simufact Forming offers five types of matrix-solving solvers, in which the simulation time and ear height were investigated. The simulation was done with two plasticity models and two hardening models.

MATERIAL AND METHODS

Materials

Research Four types of aluminum sheets were chosen for the experimental research: H11, H22, H24, and T6. The thickness of H11, H24, and H22 sheets is t0 = 0.8 mm, while type T6 has a thickness of t0 = 1 mm.
H11, H22, and H24 aluminum sheets are made of EN AW 5754 alloy (AlMg3). Type H11 is lightly strain-hardened, H22 is strain-hardened and partially annealed to ¼ hard, and sheet H24 is strain-hardened and partially annealed to ½ hard. T6 aluminium sheet belongs to the EN AW 6082 (AlSi1MgMn) group and undergoes heat treatment to achieve steady states after dissolution annealing and subsequent artificial ageing. **Tables 1** and **2** display the chemical composition of examined alloys. **Table 3** shows the declared mechanical properties of these aluminum sheets.
Experimental testing occurred within the Laboratory of Testing Mechanical Properties, part of the Department of Technology, Materials, and Computer-Aided Support. Material properties were tested according to the standard STN EN ISO 6892-1:2020, normal anisotropy ratio according to STN EN ISO 10113: 2020, and strain-hardening exponent according to STN EN ISO 10275: 2021. The hydraulic testing machine TIRAtest2300 is shown in **Fig. 1**. Five samples were produced and tested at 0 °, 45 °, and 90 ° in the rolling direction to measure the values of mechanical and formability properties. The extensometers measured the elongation and width of samples (TIRA Maschinenbau GmbH, Rauenstein, Germany). The obtained results from uniaxial tests are shown in **Table 4**.

Table 1 The chemical composition of alloy 5754 (AlMg3), wt. / %

	Si	Fe	Cu	Mn	Mg	Cr	Zn	Ti
Minimum					2.60			
Maximum	0.40	0.40	0.10	0.50	3.60	0.30	0.20	0.15

Table 2 The chemical composition of alloy 6082 (AlSi1MgMn), wt. / %

	Mn	Fe	Mg	Si	Cu	Zn	Ti	Cr
Minimum	0.40		0.60	0.70				
Maximum	1.00	0.50	1.20	1.30	0.10	0.20	0.10	0.25

Table 3 The mechanical properties of tested aluminum alloys sheets

Properties	H11	H22	H24	T6
Yield Strength R_e	60 MPa	130 MPa	160 MPa	250 MPa
Tensile Strength R_m	160 – 200 MPa	220 – 270 MPa	240 – 280 MPa	295 MPa
Ductility A_{80}	12 %	7 %	6 %	6 %
Hardness HBW	44 HB	63 HB	70 HB	95 HB

Fig. 1 Hydraulic testing machine TIRAtest2300

Five samples were produced and tested at 0 °, 45 °, and 90 ° in the rolling direction to measure the values of mechanical and formability properties. The extensometers measured the elongation and width of the samples (TIRA Maschinenbau GmbH, Rauenstein, Germany). **Fig. 2** shows the test samples of material H22 after the uniaxial tensile test.

Fig. 2 Test samples of material H22 after uniaxial tensile test, RD = 90 °

Fig. 3-7 illustrate the mechanical properties of different materials obtained from uniaxial tensile tests in three directions (0 °, 45 °, 90 °) concerning the rolling direction. The measured values show that the yield strength values for materials H22, H24, and T6 exhibit slight variations depending on the rolling direction. In contrast, material H11 demonstrates higher anisotropy in yield strength.

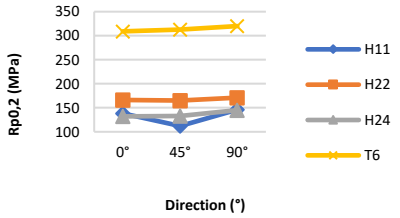

Fig. 3 Dependence of $R_{p0.2}$ in 0 °, 45 °, 90 ° directions with respect to the rolling direction for all examined materials

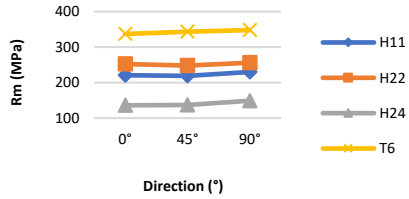

Fig. 4 Dependence of R_m in 0 °, 45 °, 90 ° directions concerning the rolling direction for all examined materials.

As presented in **Fig. 4**, ultimate tensile strength results show minimal anisotropy across all examined materials.
Ductility (A_{80}), shown in **Fig. 5**, exhibits substantial anisotropy in most of the examined materials.

Likewise, the normal anisotropy ratio, depicted in **Fig. 6**, indicates a planar anisotropy. This ratio is significant in terms of the formability of aluminum sheets, determining their resistance to thinning and suitability for deep drawing.

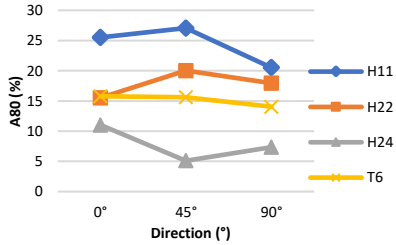

Fig. 5 Dependence of A_{80} in 0 °, 45 °, 90 ° directions with respect to the rolling direction for all examined materials.

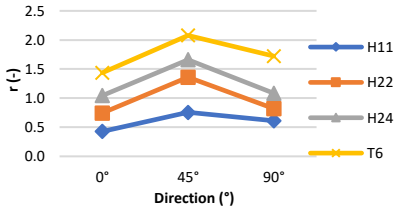

Fig. 6 Normal anisotropy ratio in 0 °, 45 °, 90 ° directions concerning the rolling direction for all examined materials.

The strain hardening exponent (see **Fig. 7**) is a criterion used to evaluate the suitability of sheets for deep drawing. Minimal anisotropy of the strain hardening exponent was found in all examined materials.

Table 4 The mechanical properties of the aluminum alloys obtained from the uniaxial tensile test

RD (°)	Material	$R_{p0.2}$ (MPa)	R_m (MPa)	A_{80} (%mm)	r (-)	r_m (-)	n (-)	n_m (-)
0		138	221	25.53	0.428		0.099	
45	**H11**	112	219	27.07	0.757	0.598	0.098	0.098
90		146	230	20.52	0.609		0.098	
0		166	252	15.52	0.745		0.204	
45	**H22**	165	248	20.03	1.360	0.976	0.211	0.206
90		171	256	17.95	0.823		0.205	
0		132	136	11.03	1.045		0.140	
45	**H24**	133	137	5.10	1.660	1.264	0.142	0.141
90		145	149	7.35	1.086		0.141	
0		309	337	15.78	1.437		0.294	
45	**T6**	313	343	15.60	2.078	1.746	0.295	0.295
90		320	348	14.05	1.722		0.295	

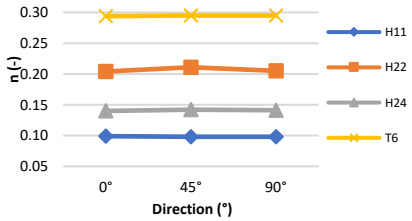

Fig. 7 The strain hardening exponent in 0 °, 45 °, 90 ° directions with respect to the rolling direction for all examined materials

Experimental procedure

The experiment consists of a cupping test conducted on hydraulic press ZD-40 (**Fig. 8a**). A specialized deep drawing tool (**Fig. 8b**) was created to assess anisotropy demonstrated by the earring on the cups. The punch radially deep draws the blank into a forming die. A mechanical blank holder applies pressure to prevent sheets from wrinkling.

a) b)

Fig. 8 a) Hydraulic press ZD-40, b) experimental deep-drawing tool

Table 5 displays the dimensions of the deep-drawing tools used in the experimental testing. For materials with a thickness of t_0 = 0.8 mm, a punch with a diameter of 31.80 mm was employed, while for t_0 = 1.0 mm, a punch with a diameter of 31.40 mm was used.

Table 5 Deep-drawing tool dimensions

Parameters	Dimensions (mm)
Punch diameter	31.80/31.40
Die diameter	33.80
Die radius	4.75
Punch radius	4.50
Clearence between punch and die	2

A deep-drawing tool was designed to evaluate anisotropy expressed by the earing of aluminum sheet cups. A mechanical blank holder applies pressure to prevent sheets from wrinkling. The punch radially deep draws the blank into a forming die. The cup test was realized for cylindrical cups. Experimental materials were used to create circular blanks with a diameter of 55 mm. The blank holding force was set to 1.2 kN. Blanks were prepared using hydraulic shears LVD CS6/31.
These blanks were used to draw three cylindrical flat-bottomed cups. The height of each cup was measured at eight points around their circumference, as illustrated in **Fig. 9a**. These measurements were taken two times in the 0 ° direction, four times in the 45 ° direction, and two times in the 90 ° direction (**Fig. 9b**). **Fig. 10** shows cylindrical cups drawn using a deep-drawing tool on a ZD-40 machine.

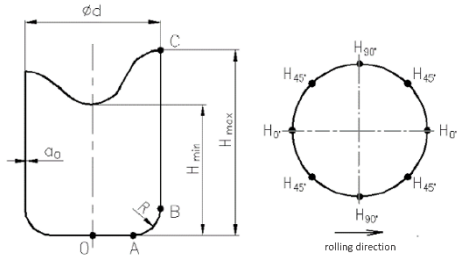

a) b)

Fig. 9 a) Earing phenomenon on cylindrical cup b) heigh measurement around circumference

Fig. 10 Cylindrical cups after cupping test

The average measured heights of the cups for examined materials are shown in the **Table 6**.

Table 6 Average heights of the cups after the cupping test (mm)

Mat.	0 °	45 °	90 °	135 °	180 °	225 °	270 °	315 °
H11	16.62	18.53	16.95	18.97	16.69	18.70	17.13	19.01
H22	17.18	17.30	16.47	17.50	17.39	18.04	17.68	18.45
H24	16.46	19.03	16.48	21.31	16.75	21.00	17.08	19.55
T6	17.85	18.30	16.70	18.54	18.05	19.54	18.68	19.59

From the measured values, the following parameters were calculated - mean ear height ΔH (1), ear height expressed as a percentage Z (2), Δh, the maximum difference between the measured heights (3), and the mean height h_{avg} (4).

$$\Delta H = \frac{1}{2}(h_0 - 2h_{45} + h_{90}) \quad (mm) \quad (1.)$$

$$Z = \frac{h_{max} - h_{min}}{h_{min}} \cdot 100 \quad (\%) \quad (2.)$$

$$\Delta h = h_{max} - h_{min} \quad (mm) \quad (3.)$$

$$h_{avg} = \frac{\sum h_{max} + \sum h_{min}}{8} \quad (mm) \quad (4.)$$

Table 7 shows the values calculated according to the relations (1-4).

Table 7 Earing values of tested aluminum alloys sheets

Samples	ΔH (mm)	Z (%)	Δh (mm)	h_{avg} (mm)
H11	- 1.75	14.38	2.39	17.83
H22	-0.47	12.02	1.98	17.50
H24	- 2.56	27.58	4.52	18.46
T6	- 1.02	17.30	2.89	18.41

The values obtained from the cup test are shown in **Fig. 11**.

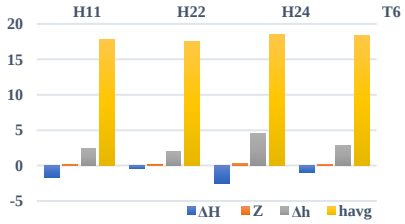

Fig. 11 Earing parameters obtained from cupping test

It can be concluded that the evaluated H24 type sheet has the highest values of all measured variables compared to H11, H22 and T6 sheets. This indicates that the most anisotropic aluminum sheet is the H24 material. The value of 4.52 mm indicates the difference between the maximum and minimum values of the measured heights.

Simulation setup

The numerical simulations of deep drawing were conducted using CAE forming software Simufact Forming based on MSC´s implicit Marc solver. Tool geometry is an important factor in sheet metal forming. Thus, it is also important to correctly model forming tools which are then used in CAE software. The imported CAD model of the experimental tool (to reduce the simulation time, a quarter of the circular tool was chosen), which was used in numerical simulation, is pictured in **Fig. 12a**. The geometry and dimensions of the CAD model of the tool and materials were the same as in the experiment (**Table 5**). After importing the CAD model into the CAE environment, the blank sheets needed for simulation meshed with hexahedral solid elements (**Fig. 12b**). If a strain limit of 0.2 was reached, the software meshed the model.

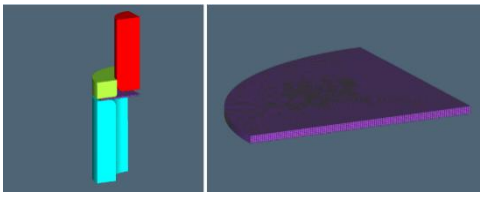

a) b)

Fig. 12 a) CAD model of deep-drawing tool, b) mesh for the blank.

The investigated parameter was the ear height of cups made from various materials while applying a blank holding force of 1.2 kN. The simulations applied the anisotropic Hill48 and Barlat models with isotropic hardening models based on Holomon and Krupkowski. A numerical simulation was conducted with a coefficient of friction of 0.1, using the Coulomb friction law.
The numerical simulation was performed for all examined materials under the same conditions (punch velocity, friction coefficient, die and punch radius and clearance between die and punch). The primary objective of this simulation was to determine earing values for the cups made from experimental materials using different anisotropic and strain hardening models and then compare these values with experimental results. The numerical simulation results are presented in **Fig. 13-16** and were subsequently compared with values obtained during the experimental test (refer to **Fig. 17-20**).

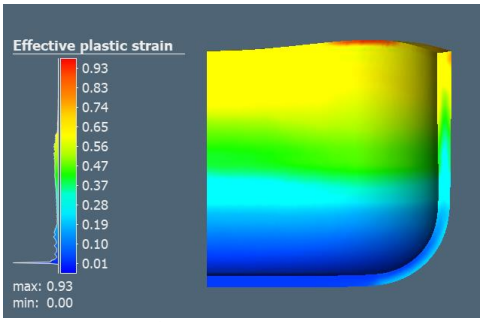

Fig. 13 Simulation of H11 material using Hill-Hollomon models

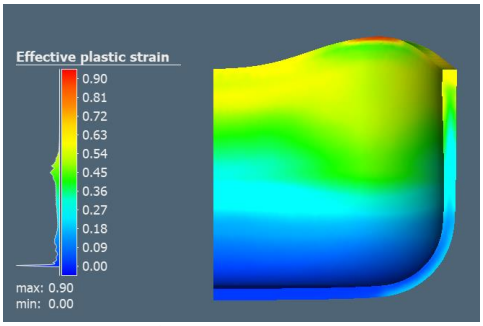

Fig. 14 Simulation of H22 material using Hill-Hollomon models

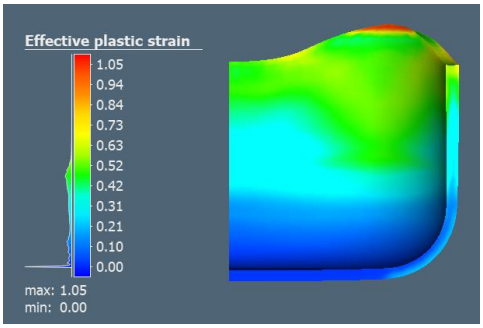

Fig. 15 Simulation of H22 material using Hill-Hollomon models

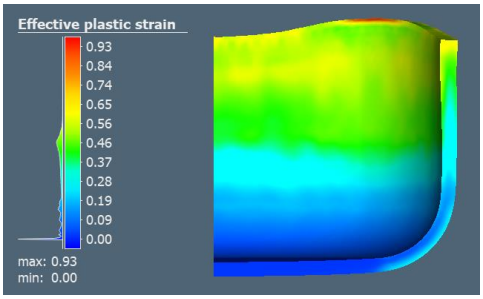

Fig. 16 Simulation of T6 material using Hill-Hollomon models

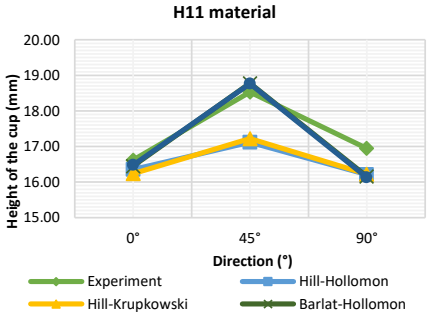

Fig. 17 Earing parameters obtained from cup test and numerical simulation for material H11

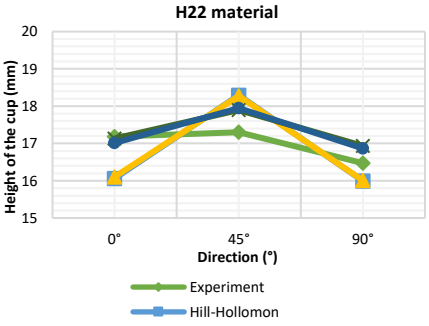

Fig. 18 Earing parameters obtained from cup test and numerical simulation for material H22

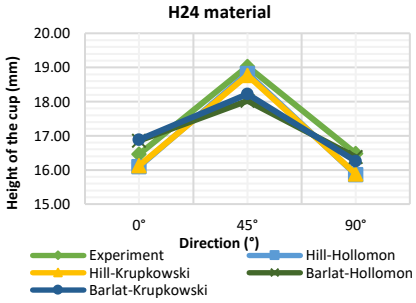

Fig. 19 Earing parameters obtained from cup test and numerical simulation for material H26

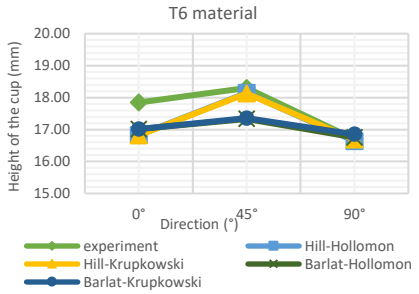

Fig. 20 Earing parameters obtained from cup test and numerical simulation for material T6

The relationship between the number of elements and the quality and simulation time was verified within the simulation. Individual simulations were performed on T6 material (t_0 = 1 mm) with various elements per sheet thickness: 3, 5, 7, 9, and 11 elements per thickness. The model of deep-drawing tool and parameters remained unchanged. The anisotropic Hill48 model was used in combination with the Hollomon hardening model. **Fig. 21** shows the measured heights of the ears and compares them with the results of the conducted experiment. **Table 8** displays the deviations in heights (in mm) from the experiment's results.

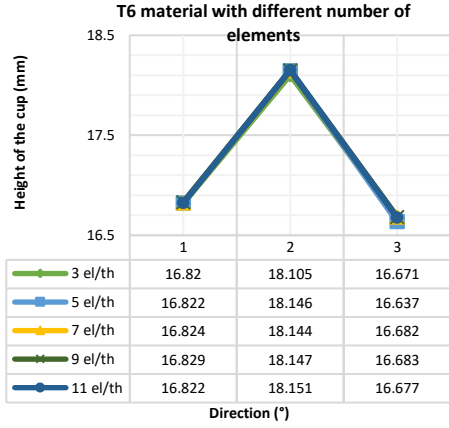

	1	2	3
3 el/th	16.82	18.105	16.671
5 el/th	16.822	18.146	16.637
7 el/th	16.824	18.144	16.682
9 el/th	16.829	18.147	16.683
11 el/th	16.822	18.151	16.677

Fig. 21 Earing parameters obtained from cup test and numerical simulation for material T6 with different number of elements (el/th – elements per thickness)

Table 8 Height deviations compared to the experiment (mm)

RD	Experiment	3 el./th.	5 el./th.	7 el./th.	9 el./th.	11 el./th.
0 °	17.85	-1.03	-1.028	-1.026	-1.021	-1.021
45 °	18.3	-0.195	-0.154	-0.156	-0.153	-0.149
90 °	16.7	-0.029	-0.063	-0.018	-0.017	-0.023

The complexity of simulation calculations increases with a higher number of elements per sheet thickness. The representation of simulation computational times is shown in **Fig. 22**. Simufact Forming offers five types of solvers for matrix solving. The default solver for sheet metal forming within Simufact Forming is the Automatic solver. In addition to this solver, other solvers are also available, suitable for sheet metal forming simulations.

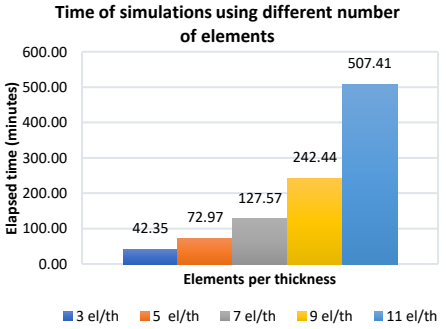

Fig. 22 Computational times of the simulations using different number of elements

Simufact Forming provides the following recommendations when choosing a solver:
Pardiso Direct Sparse: A reliable direct solver suitable for models of various sizes. It is compatible with all element types and particularly useful for unstable processes.
Multifrontal Sparse: Direct solver well-suited for small and medium-sized models, supporting all element types. It is especially advantageous for handling unstable processes.
MUMPS Parallel Direct: Specifically designed for handling large models and optimized for parallelization.
Iterative Sparse: Requires little memory and is applicable for larger models. This solver is not the best choice for simulating rigid-plastic material behavior due to the incompressibility boundary conditions.

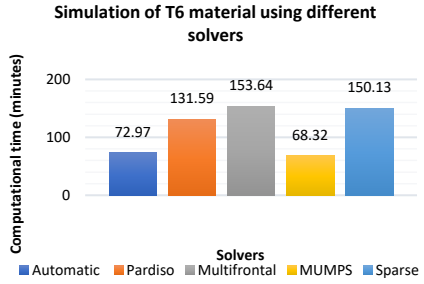

Fig. 23 Simulation of T6 material using different solvers

The experiment involved the utilization of different solvers for simulating the deep-drawing process of T6 material with a 1 mm thickness. Effects of different solvers on computational time were examined. The simulation parameters and tool dimensions were unchanged. An anisotropic Hill48 model combined with the Hollomon hardening model was employed. The sheet model was discretized using solid hexahedral elements with the size of 0.25 mm, with a density of 5 elements per sheet thickness. **Fig. 23** shows the computational time of simulations.

RESULTS AND DISCUSSION

From the experience of aluminum sheet manufacturers, as well as from our long-standing experience focused on the formability research of thin sheets, we can clearly state that aluminum alloy sheets do not behave identically to thin steel sheets used in deep drawing [13, 16]. Due to specific properties of aluminum alloys sheets (lower yield strength, lower tensile strength, and different surface microgeometry), these sheets are much more susceptible to changes (especially to change the friction parameters) than thin steel sheets during deep drawing. The fact that most aluminum sheets have a significantly lower hardness than steel sheets means that the frictional conditions in the tool often lead to the formation of built-ups, particularly on the die edges, which increase the coefficient of friction during drawing.
For the experimental research, four different aluminum alloys were used. Mechanical and plastic properties were different for examined aluminum sheets. Obtained results from uniaxial tensile test showed that the anisotropy of yield strength is lower for all materials except H11. The tensile strength of all the materials used showed minimal anisotropy. The ductility A_{80} showed a higher anisotropy for all materials. Normal anisotropy ratio showed the highest value for all examined sheets in the 45 ° direction with respect to the rolling direction. The strain hardening exponent did not show anisotropy.
The results from the experimental cup test showed that despite the different mechanical properties of the examined sheets, the height of ears (see Table 6) is approximately same with only small variations. For all examined materials, the ears formed in the directions of 45 °, 135 °, 225 ° and 315 ° with respect to the rolling direction.
Fig. 24 shows the most common errors that occur when drawing circular cups from aluminum sheets. These errors are caused by the change in friction ratios in the drawing tools. Due to the changes of friction parameters, a non-uniform drawing of material from the flange occurred. This resulted in different cup heights without showing signs of anisotropy (no earrings). This phenomenon occurs especially at low blank holding pressures.

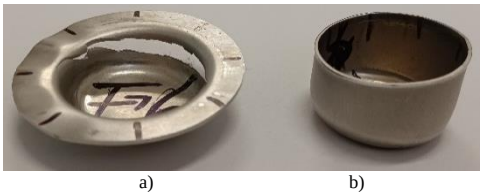

a) b)

Fig. 24 Frequent errors when drawing cups from aluminum sheets, a) rupture of the cup due to uneven holding force and b) unequal height of the cup due to a change in friction ratios

The experimental results of the drawing process were compared with the simulation results using the Simufact Forming software, which is based on MSC's implicit Marc solver. The deep drawing simulation utilized the anisotropic Hill48 and Barlat models and isotropic hardening models based on Holomon and Krupkowski.

The simulation results show that for material H11, the experiment exhibited higher earing in all directions compared to the simulation.

In the case of material H22, the experimentally measured earing was minimal. However, the resulting earning was significantly higher for all combinations of models used in the simulation, with the most significant difference observed in simulations using the Hill-Krupkowski and Hill-Hollomon models.

Material H24 showed the best consistency between the Hill-Krupkowski and Hill-Hollomon models and the experimental results.

For material T6, the experimental results varied from the simulation only in the 0° direction, with an ear height difference of 1 mm. This difference may be attributed to changes in friction ratios within the tool during the experiment.

Different numbers of elements (3, 5, 7, 9, and 11) were selected for T6 material with a 1 mm thickness to compare simulation results with experiments. Tool dimensions and parameters remained unchanged. The Hill48 model was employed with the Hollomon hardening model for the simulation.

Fig. 21 and **Table 8** show that the number of selected elements had no impact on the calculation's accuracy; the ear height remained consistent across all element numbers. However, the number of elements significantly affected the simulation time, as shown in **Fig. 22**. When the number of elements was increased from 3 to 11, the simulation time was 12 times longer. Compared to 9 elements, it was 2 times longer. These results indicate that increasing the number of elements does not impact the accuracy of ear height but significantly extends simulation time.

In another comparison between simulation and experiment, the simulation results from the Simufact Forming program were evaluated using five different solvers. The simulation times for all five solvers offered by the software are displayed in **Fig. 23**. The shortest simulation time in minutes was achieved using the MUMPS solver, while the Automatic solver required an additional 4.5 minutes. For other solver types, the simulation times were approximately two or more times longer while maintaining the same result accuracy.

CONCLUSION

In recent years, thin aluminum alloy sheets have gained popularity in the automotive industry for their weight-reduction potential in various components. Thin aluminum sheets are commonly processed through drawing, forming cylindrical extracts such as beverage cans.

Based on the comparison of experimental and simulation results, the following conclusions can be drawn:

- The most accurate match with experimentally measured ear height was achieved through simulation using the Hill-Hollomon and Hill-Krupkowski models.
- The number of elements per material thickness does not affect the calculation of ear height when drawing aluminum alloy sheets. However, it significantly impacts simulation time, which can be up to 12 times longer with more elements.
- The choice of solver type in the Simufact Forming software substantially influences simulation time, with variations of 2 times or more when using different solvers while maintaining result accuracy.

Acknowledgments: Authors are grateful for the support of experimental works by projects APVV-21-0418 and KEGA 018TUKE-4/2024 funded by Slovak Research and Development Agency.

REFERENCES

1. L. M. Cheng, W. J. Poole, J. D. Embury, D. J. Lloyd: Metallurgical and Materials Transactions, 34, 2003, 2473–2481. https://doi.org/10.1007/s11661-003-0007-2.
2. G. Ubertalli, P. Matteis, S. Ferraris, C. Marcianò, F. D'Aiuto, M. M. Tedesco, D. De Caro: Metals, 10, 2020, 242. https://doi.org/10.3390/met10020242.
3. R. Schneider, B. Heine, R. J. Grant, Z. Zouaoui: Aluminium Sheet Metal Forming at Low Temperatures, IOP Conference Series: Materials Science Engineering, 74, 2015, 012014. https://doi.org/10.1088/1757-899X/74/1/012014.
4. P. Xiang, L. J. Jia, M. Shi, M. Wu: Engineering Fracture Mechanics, 186, 2017, 449–465. https://doi.org/10.1016/j.engfracmech.2017.11.006.
5. X. Zhao, H. Li, T. Chen, B. Cao, X. Li: Materials, 12, 2019, 2064. https://doi.org/10.3390/ma12132064.
6. S. K. Shaha, F. Czerwinski, W. Kasprzak, J. Friedman, D. L. Chen: Metallurgical and Materials. Transactions, 46, 2015, 3063–3078. https://doi.org/10.1007/s11661-015-2880-x.
7. EN 573-3:2019-12. *Aluminum and Aluminum Alloys-Chemical Composition and Types of Wrought Products-Part 3*: Chemical Composition and Types of Articles; European Committee for Standardization: Brussels, Belgium, 2019.
8. EN 1706:2020-10. *Aluminium and Aluminium Alloys. Castings*. Chemical Composition and Mechanical Properties; European Committee for Standardization: Brussels, Belgium, 2020.
9. T. Kvačkaj et al.: Materials Science Forum, 633-634, 2010, 273-302. https://doi.org/10.4028/www.scientific.net/MSF.633-634.273.
10. P. Wagner, H. J. Brinkman, E. Bruenger, S. Keller: Proc. *New Developments in Sheet Metal Forming*, Germany, Ed. M. Liewald, DGM, Fellbach-Stuttgart, 2008.
11. C. Lahaye, J. Hirsch, D. Bassan, B. Criqui, Ch. Sahr, M. Goede: Contribution of aluminium to the multi-material lightweight BIW design of SuperLight-Car. *11th International Conference on Aluminium Alloys*. Aachen, Germany, 2008.
12. J. Mucha, Ľ. Kaščák, W. Witkowski: Materials, 14 (1), 2021, 2980. https://doi.org/10.3390/ma14112980.
13. T. Trzepiecinski: Acta Metallurgica Slovaca, 26, 2020, 42–44. https://doi.org/10.36547/ams.26.2.553.
14. P. Mulidrán, E. Spišák, M. Tomáš, J. Majernikova, J. Varga: Acta Metallurgica Slovaca, 27, 2021, 103–108. https://doi.org/10.36547/ams.27.3.899.
15. A. Kubit, T. Trzepieciński, B. Krasowski, J. Slota, E. Spišák: Materials, 13(13), 2020, 2929. https://doi.org/10.3390/ma13132929.
16. J. Slota, M. Jurčišin, E. Spišák: Key Engineering Materials, 586, 2014, 245-248. https://doi:10.4028/www.scientific.net/KEM.586.245.
17. P. Mulidrán et al.: Materials, 16(2), 2023, 811. https://doi.org/10.3390/ma16020811.
18. J. W. Yoon, R. E. Dick, F. Barlat: International Journal of Plasticity, 27, 2011, 1165–1184. https://doi.org/10.1016/j.ijplas.2011.01.002.
19. K. Chung, D. Kim, T. Park: European Journal of Mechanics, A/Solids, 30, 2011, 275–280. https://doi.org/10.1016/j.euromechsol.2011.01.006.
20. S. Panich, V. Uthaisangsuk, S. Suranuntchai, S. Jirathearanat: Key Engineering Materials, 504, 2012, 89–94. https://doi.org/10.4028/www.scientific.net/KEM.504-506.89.

21. L. Wang, T. C. Lee: International Journal of Machine Tools and Manufacture, 46, 2006, 988–995. https://doi.org/10.1016/j.ijmachtools.2005.07.050.
22. S. Soare, J. W. Yoon, O. Cazacu, F. Barlat: Applications of a Recently Proposed Anisotropic Yield Function to Sheet Forming. *Advanced Methods in Material Forming*, Springer: Berlin, 2007, 131–149. https://doi.org/10.1007/3-540-69845-0_8.
23. F. Barlat, H. Aretz, J. W. Yoon, M. E. Karabin, J. C. Brem, R. E. Dick: International Journal of Plasticity, 21, 2005, 1009–1039. https://doi.org/10.1016/j.ijplas.2004.06.004.
24. P. D. Barros, J. L. Alves, M. C. Oliveira, L. F. Menezes: International Journal of Solids and Structures, 151, 2018, 135–144. https://doi.org/10.1016/j.ijsolstr.2017.06.034.
25. N. Younas, H. Chalal, F. Abed-Meraim: Procedia Manufacturing, 47, 2020, 1416–1423. https://doi.org/10.1016/j.promfg.2020.04.302.
26. H. B. Wang, M. Wan, Y. Yan, et al.: Journal of Mechanical Engineering, 49(24), 2013, 45-53. https://doi.org/10.3901/JME.2013.24.045.
27. Y. Sun, C. Z. Chi, L. C. Li, et al.: Journal of Plasticity Engineering, 24(1), 2017, 85-91. https://doi.org/10.1007/s00170-016-8816-9.
28. H. B. Wang, M. L. Men, Y. Yan, et al.: Journal of Mechanical Engineering, 54(24), 2018, 77-87. https://doi.org/10.3901/JME.2018.24.077.
29. M. Athale, A. K. Gupta, S. K. Singh, et al.: International Journal of Material Forming, 2017 (2013), 1-12. https://doi.org/10.1007/s12289-017-1358-3.
30. R. A. Hill: Proceedings of the Royal Society A, 193(1033), 1948, 281-297. https://doi.org/10.1098/rspa.1948.0045.
31. B. T. Tang, Y. S. Lou: Acta Mechanica Solida Sinica, 32(1), 2019, 50-68. https://doi.org/10.1007/s10338-018-0043-5.
32. S. Bagherzadeh, M. J. Mirnia, B. Mollaei Dariani: Journal of Manufacturing Processes, 18, 2015, 131-140. https://doi.org/10.1016/j.jmapro.2015.03.004.
33. K. E. N'souglo, J. A. Rodríguez-Martínez, A. Vaz-Romero, et al.: International Journal of Solids and Structures, 159, 2019, 272-288. https://doi.org/10.1016/j.ijsolstr.2018.10.006.
34. H. B. Wang, Y. Yan, M. Wan, et al.: International Journal of Solids and Structures, 49(26), 2012, 3693-3710. https://doi.org/10.1016/j.ijsolstr.2012.08.007.
35. Y. Yan, H. B. Wang, Q. Li: Journal of Manufacturing Processes, 20, 2015, S1526612515001061. https://doi.org/10.1016/j.jmapro.2015.09.009.
36. D. M. Neto, M. C. Oliveira, J. L.: Materials & Design, 60, 2014, 368-379. https://doi.org/10.1016/j.matdes.2014.04.008.
37. F. Barlat, J. C. Brem, J. W. Yoon, et al.: International Journal of Plasticity, 19(9), 2003, 1297-1319. https://doi.org/10.1016/S0749-6419(02)00019-0.
38. Y. Yan, C. Wu, Z. L. Hu, et al.: Journal of Plasticity Engineering, 23(2), 2016, 92-97. https://doi.org/10.3969/j.issn.1007-2012.2016.02.016.
39. E. H. Lee, B. S. Thomas, J. W. Yoon: International Journal of Plasticity, 99(1), 2017, 120-143. https://doi.org/10.1016/j.ijplas.2017.08.007.
40. J. Noder, A. Abedini, T. Rahmaan, et al.: IOP Conference Series Materials Science and Engineering, 418(1), 2018, 012019. https://doi.org/10.1088/1757-899X/418/1/012019.
41. Y. Shi, H. Jin, P. D. Wu: European Journal of Mechanics - A/Solids, 69, 2018, 1-11. https://doi.org/10.1016/j.euromechsol.2017.11.013.
42. H. Fukumasu, T. Kuwabara, H. Takizawa: Journal of Physics Conference Series, 734(3), 2016, 032022. https://doi.org/10.1088/1742-6596/734/3/032022.
43. K. Chung, K. Shah: International Journal of Plasticity, 8, 1992, 453-476. https://doi.org/10.1016/0749-6419(92)90059-L.
44. J. W. Yoon, F. Barlat, K. Chung, F. Pourboghrat, D. Y. Yang: Journal of Materials Processing Technology, 80-81, 1998, 433-437. https://doi.org/10.1016/S0924-0136(98)00148-4.
45. J. W. Yoon, F. Barlat, K. Chung, F. Pourboghrat, D. Y. Yang: International Journal of Plasticity, 16, 2000, 1075-1104. https://doi.org/10.1016/S0749-6419(99)00086-8.
46. J. W. Yoon, F. Barlat, R. E. Dick, M. E. Karabin: International Journal of Plasticity, 22, 2006, 174-193. https://doi.org/10.1016/j.ijplas.2005.03.013.
47. J. H. Yoon, O. Cazacu, J. W. Yoon, R. E. Dick: International Journal of Mechanical Science, 52, 2010, 1563-1578. doi: 10.1016/j.ijmecsci.2010.07.005
48. I. N. Vladimirov, M. Schwarze, S. Reese: GAMM Mitteilungen, 33, 2010, 116-129. https://doi.org/10.1002/gamm.201010009.
49. S. Chatti, N. Chtioui: European Journal of Computational Mechanics, 20, 2011, 427-453. https://doi.org/10.3166/ejcm.20.427-453.
50. M. Vrh, M. Halilovic, B. Starman, B. Stok, D. S. Comsa, D. Banabic: European Journal of Mechanics A/Solids, 45, 2014, 59-74. https://doi.org/10.1016/j.euromechsol.2013.11.013.
51. T. Park, K. Chung: International Journal of Solids and Structures, 49(25), 2012, 3582–3593. https://doi.org/10.1016/j.ijsolstr.2012.02.015.
52. K. B. Othmen, K. Sai, P. Y. Manach, K. Elleuch: Journal of Materials: Design and Application, 233, 2019, 699-713. https://doi.org/10.1177/1464420717701950.
53. T. J. Grillo, R. A. F. Valente, R. J. Alves de Souza: International Journal of Material Forming, 8, 2015, 533-547. https://doi.org/10.1007/s12289-014-1176-9.
54. S. Izadpanah, S. H. Ghaderi, M. Gerdooei: International Journal of Mechanical Sciences, 115-116, 2016, 552-563. https://doi.org/10.1016/j.ijmecsci.2016.07.036.
55. Z. Feng, S. Y. Yoon: Journal of Manufacturing Processes, 33, 2018, 256-267. https://doi.org/10.1016/j.jmapro.2018.05.003.
56. J. Mucha, Ľ. Kaščák, E. Spišák: Archives of Civil and Mechanical Engineering, 11, 2011, 135-148. https://doi.org/10.1016/S1644-9665(12)60179-4.
57. A. M. Habraken, T. A. Aksen, J. L. Alves, et al.: International Journal of Material Forming, 15, 2022, 61. https://doi.org/10.1007/s12289-022-01672-w.